OXFORD

Human Molecular Genetics, 2022, Vol. 31, 8, 1325–1335
https://doi.org/10.1093/hmg/ddab323
Advance access publication date 5 November 2021
Original Article

Molecular alterations due to *Col5a1* haploinsufficiency in a mouse model of classic Ehlers–Danlos syndrome

Keren Machol[1], Urszula Polak[1], Monika Weisz-Hubshman[1], I-Wen Song[1], Shan Chen[1], Ming-Ming Jiang[1], Yuqing Chen-Evenson[1], Mary Ann E. Weis[2], Douglas R. Keene[3], David R. Eyre[2] and Brendan H. Lee[1,*]

[1]Department of Molecular and Human Genetics, Baylor college of Medicine, Houston, TX 77030, USA
[2]Department of Orthopedics and Sports Medicine, University of Washington Seattle, WA 98195, USA
[3]Micro-Imaging Center, Shriners Hospital for Children, Portland, OR 97239, USA

*To whom correspondence should be addressed at: Department of Molecular and Human Genetics, Baylor college of Medicine, Houston, TX 77030, USA. Tel: +1 (713) 798 5443; Fax: +1 (713) 798 5168; Email: Blee@bcm.edu

Abstract

Type V collagen is a regulatory fibrillar collagen essential for type I collagen fibril nucleation and organization and its deficiency leads to structurally abnormal extracellular matrix (ECM). Haploinsufficiency of the *Col5a1* gene encoding α(1) chain of type V collagen is the primary cause of classic Ehlers–Danlos syndrome (EDS). The mechanisms by which this initial insult leads to the spectrum of clinical presentation are not fully understood. Using transcriptome analysis of skin and Achilles tendons from *Col5a1* haploinsufficient (*Col5a1*$^{+/-}$) mice, we recognized molecular alterations associated with the tissue phenotypes. We identified dysregulation of ECM components including thrombospondin-1, lysyl oxidase, and lumican in the skin of *Col5a1*$^{+/-}$ mice when compared with control. We also identified upregulation of transforming growth factor β1 (Tgf-β) in serum and increased expression of pSmad2 in skin from *Col5a1*$^{+/-}$ mice, suggesting Tgf-β dysregulation is a contributor to abnormal wound healing and atrophic scarring seen in classic EDS. Together, these findings support altered matrix to cell signaling as a component of the pathogenesis of the tissue phenotype in classic EDS and point out potential downstream signaling pathways that may be targeted for the treatment of this disease.

Introduction

Classic type Ehlers–Danlos syndrome (EDS) is a rare connective tissue disorder involving mainly skin and tendons with hyperextensible and fragile skin, delayed wound healing, atrophic scars and hypermobile joints. The multisystemic phenotype includes musculoskeletal pain, muscle weakness, blood vessels fragility, and rare involvement of the cardiovascular system, which usually results in minor clinical consequences (1). The current clinical management of classic EDS is symptomatic and focuses on skin and joints complications. Classic EDS is caused mostly by pathogenic variants in genes *COL5A1* and *COL5A2* encoding the main two chains [pro-α1(V) and pro-α2(V)] of collagen V heterotrimer, respectively. Although multiple types of pathogenic variants were identified in both genes in patients with classic EDS, haploinsufficiency of α1(V) collagen is the most frequent underlying mechanism that leads to the classic EDS phenotype (2).

Type V collagen (ColV) is a regulatory fibril-forming collagen, which is a quantitatively minor component of the total collagen in multiple connective tissues including skin, tendon, and bone (3). ColV is critical for nucleation and regulation of lateral expansion of type I collagen fibrils (4). ColV retains its amino-terminal pro-peptide after incorporation into collagen fibrils. The amino-terminus projects between type I collagen molecules on the fibril surface and inhibits its lateral expansion (3). Fibroblasts with ColV haploinsufficiency show no change in their type I collagen synthesis rate compared with control fibroblasts but fibril diameter is larger, and the number of fibrils assembled is reduced (5,6). A *Col5a1* haploinsufficient mouse model generated by Wenstrup *et al.* (*Col5a1*$^{+/Neo}$) was shown to recapitulate the skin phenotype of patients with classic EDS presenting hyperextensible skin and reduced tensile strength of both wounded and unwounded skin. Collagen fibril density in the skin of *Col5a1*$^{+/Neo}$ mice was low with large diameter fibrils and low content of ColV (4). Analysis of tendons from *Col5a1*$^{+/Neo}$ revealed diminished healing of the patellar tendon after injury, decreased dynamic response properties of the tendon and abundance of large diameter collagen fibrils in the tendons compared with wild-type controls (7,8). Mice with tendons and ligaments specific deletion of *Col5a1* recapitulated the joint phenotype seen in classic EDS patients and demonstrated altered fibril structure with increased fibril diameters and decreased fibril number (9).

Col5a1$^{+/Neo}$ mice demonstrated a delay in dermal collagen accumulation between 4 and 8 weeks of age. Yet, by the age of 12 weeks, the collagen content in their skin was comparable to controls. The abnormal skin phenotype was detectable even after normalization of skin collagen content (6). This suggests activation of efficient compensatory mechanisms to overcome

Received: July 29, 2021. **Revised:** October 7, 2021. **Accepted:** October 29, 2021

the reduced collagen content in the skin and that this transient collagen deficiency is not the only contributor to the phenotype. Fibroblasts from *Col5a1*$^{+/Neo}$ *mice* have reduced proliferation and reduced attachment to collagen I, III and fibronectin (10). Moreover, in yeast two-hybrid screen, ColV *N*-propeptide was demonstrated to bind multiple extracellular components including α1(I)- and α2(I)-collagen chains, α1(VI)-, α2(VI)- and α3(VI)-collagen chains, tenascin-C, fibronectin, procollagen C-proteinase enhancer-1 (PCPE-1), tissue inhibitor of metalloproteinases-1 (TIMP-1), MMP-2 (matrix metalloproteinase 2) and TGF-β1 (transforming growth factor β1) (11). *In vitro* studies in *COL5A1* haploinsufficient human fibroblasts demonstrated abnormal extracellular matrix (ECM) organization with reduced levels of the major ECM component fibronectin and alterations in collagen and fibronectin receptors including a reduction in collagen I receptor $\alpha_2\beta_1$ integrin and preference of the minor fibronectin receptor $\alpha_V\beta_3$ integrin, which is expressed in normal fibroblasts during wound healing over the canonical fibronectin receptor, $\alpha_5\beta_1$ integrin (12). $\alpha_V\beta_3$ integrin is thought to enhance cell adhesion and prevent anoikis in the abnormal ECM in classic EDS (13). Although reduced expression of ColV is at the basis of the pathophysiology of classic EDS, the underlying molecular consequences are not fully understood.

Here, we aim to identify molecular consequences downstream of *Col5a1* haploinsufficiency in the *Col5a1*$^{+/Neo}$ mouse model while also validating the phenotypic features in a second model generated by CRISPR/Cas9 and without residual selectable neomycin cassettes that might have off-target effects. To find common mechanisms among different tissues, we performed transcriptomic analysis of both skin and Achilles tendons of *Col5a1* haploinsufficient mice compared with controls and distinguished differentially expressed genes (DEGs) that are associated with classic EDS.

Results

Transcriptome analysis of skin and Achilles tendons in *Col5a1*$^{+/Neo}$ mice

To determine the global transcriptional alterations associated with *Col5a1* haploinsufficiency, we performed RNAseq using RNA extracted from skin and Achilles tendons of *Col5a1*$^{+/Neo}$ mice and controls. We identified a total of 30 and 140 DEGs in the skin and the tendons of *Col5a1*$^{+/Neo}$ mice when compared with control, respectively (Fig. 1A). In skin, the expression of 25 genes (83.3%) was upregulated and of 5 genes (16.6%) was downregulated when compared with control mice skin. In the Achilles tendon, the expression of 73 genes (52%) was upregulated and of 67 genes (48%) was downregulated when compared with controls. Five genes were differentially expressed in both tissues with expression of three of these genes changed in a similar direction, and expression of two genes changed in opposite directions. *F13a1* (coagulation factor XIII a) and *Lum* (Lumican) were upregulated in Achilles tendons and skin, whereas *Thbs1* (encoding thrombospondin-1/Tsp1) was downregulated in both. *Creb3l3* (cAMP responsive element-binding protein 3 like 3) and *Mfap4* (microfibril-associated protein 4) were upregulated in skin and downregulated in tendons.

Despite the small number of DEGs in skin and tendons (Fig. 1B), molecular pathway analysis (ingenuity pathway analysis) identified 'connective tissue disorders' and 'organismal injury and abnormalities' to be at the top relevant pathways in both tissues. Among the predicted top upstream regulators in the skin, we identified the profibrotic molecules bleomycin (14), IL13 (15) and the CC-chemokine receptor 2 (CCR2) (16) as well as the connective tissue-related microRNA, mir29 (17,18). Predicted top upstream regulators in the tendons included inflammatory regulators such as dexamethasone and the proinflammatory cytokine tumor necrosis factor. The list of DEGs in skin and tendons includes multiple genes that are associated with the ECM (Fig. 1C) including genes encoding various types of collagen, Tsp1, fibronectin, and Lum. The list also includes genes encoding ECM turnover-related enzymes such as cathepsin K (*Ctsk*) and lysyl oxidase (*Lox*), and genes associated with signaling pathways such as insulin growth factor 1 (*Igf1*) and fibroblasts growth factor receptor 4 (*Fgfr4*) in skin as well as the transcription factors scleraxis (*Scx*) and mohawk (*Mkx*) in the Achilles tendons. More than 50% (17 out of 30) of the DEGs in skin and 27% (38 out of 140) of the DEGs in the Achilles tendon were changed also in the previously reported RNA sequencing studies in a model of *Col5a1*-deficient cardiac scar tissue (19) (Fig. 1C). Interestingly, only one of the DEGs in the skin was reported to change also in cultured classic EDS human fibroblasts (20). This suggests that the results presented in this work describe the net global effects of *Col5a1* haploinsufficiency on gene expression in the tissue.

No transcriptional interference in *Col5a1*$^{+/Neo}$ mice

The *Col5a1* haploinsufficiency mouse model published by Wenstrup *et al.* (6) was generated by traditional homologous recombination inserting a neomycin expression cassette between exons 3 and 4 of *Col5a1* (*Col5a1*$^{+/Neo}$). The insertion of neomycin cassette in targeting constructs has been reported to potentially influence expression of surrounding genes that can complicate the interpretation of associated phenotype (21). To exclude potential transcriptional interference by elements of the neomycin targeting construct and to confirm the model's haploinsufficiency phenotype, we generated a second mouse model for *Col5a1* haploinsufficiency using CRISPR gene-editing technique. With single-guide RNA (sgRNA) targeting of exon 48 (out of 66 exons), we introduced a heterozygous out of frame deletion of 28 base pairs (NC_000068, position ch2:27901262, GRCm39), which leads to a premature stop codon that terminates protein translation at amino acid 1405, therefore, resulting in haploinsufficiency of *Col5a1* (*Col5a1*$^{+/\Delta}$) (Supplementary Material, Fig. S1A). Characterization of

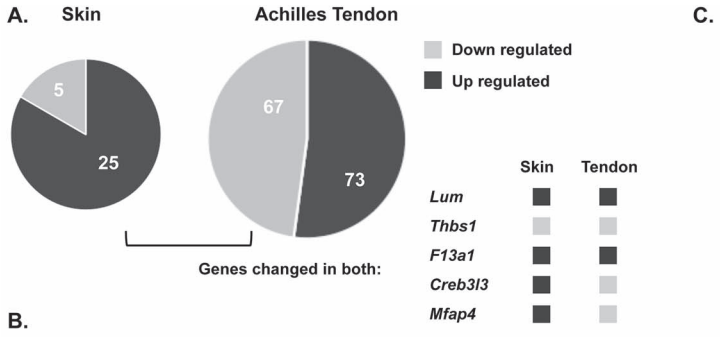

B.

Top Disease and Disorders (Skin)	p-value
Organismal Injury and Abnormalities	3.96E-03 - 1.48E-08
Respiratory Disease	2.64E-03 - 1.48E-08
Connective Tissue Disorders	3.96E-03 - 5.90E-07
Skeletal and Muscular Disorders	3.44E-03 - 5.90E-07
Cancer	3.96E-03 - 1.20E-06

Top Upstream Regulators (Skin)	p-value
Bleomycin	2.22E-07
CCR2	4.26E-07
mir-29	5.90E-06
IL13	2.24E-05

Top Disease and Disorders (Tendon)	p-value
Connective Tissue Disorders	1.28E-03 - 9.95E-13
Developmental Disorder	1.28E-03 - 9.95E-13
Hereditary Disorder	1.28E-03 - 9.95E-13
Immunological Disease	1.36E-03 - 9.95E-13
Organismal Injury and Abnormalities	1.55E-03 - 9.95E-13

Top Upstream Regulators (Tendon)	p-value
Rosiglitazone	6.2E-14
Dexamethasone	7.28E-14
TNF	6.01E-13

C.

Gene symbol	Gene description	FC in skin (p-value)	FC in tendons (p-value)	Heart scar tissue*
Col1a1	Collagen, type I, alpha 1		0.55 (0.000264)	*up*
Col1a2	Collagen, type I, alpha 2		0.576 (0.00067)	*up*
Col5a2	Collagen, type V, alpha 2	1.43 (9.33E-05)		*up*
Col11a1	Collagen, type XI, alpha 1		0.55 (0.000369)	*up*
Col11a2	Collagen, type XI, alpha 2		0.512 (3.48E-05)	*n.c.*
Col12a1	Collagen, type XII, alpha 1		0.5 (3.71E-05)	*up*
Col14a1	Collagen XIV, alpha 1	1.48 (3.16E-05)		*up*
Creb3l3	cAMP responsive element binding protein 3 like 3	1.8 (9.08E-05)	0.45 (0.00024)	*n.c.*
Ctsk	Cathepsin K	1.54 (9.11E-06)		*up*
Ecm1	Extracellular matrix protein 1		2.0 (3.72E-05)	*up*
F13a1	Coagulation factor XIII A chain	1.6 (2.97E-05)	1.86 (0.0002)	*n.c.*
Fbn2	Fibrillin 2		0.46 (6.23E-06)	*up*
Fgfr4	Fibroblast growth factor receptor 4	1.9 (0.00015)		*n.c.*
Fn1	Fibronectin 1 (glycoprotein)		2.08 (8.03E-06)	*up*
Ghr	Growth hormone receptor		1.92 (0.000127)	*n.c.*
Igf1	Insulin growth factor 1	1.5 (0.00012)		*up*
Igfals	Insulin-like growth factor binding protein, acid labile subunit		2.55 (1.24E-05)	*down*
Itga2	Integrin alpha 2 (fibronectin receptor)		0.48 (5.16E-05)	*up*
Lox	Lysyl oxidase	1.66 (1.32E-06)	0.6 (0.0018)	*up*
Loxl3	Lysyl oxidase-like 3		0.53 (0.000143)	*up*
Ltbp2	Latent transforming growth factor beta binding protein 2		2.46 (1.03E-05)	*up*
Lum	Lumican (proteglycan, SLRP)	2.1 (1.5E-14)	2.51 (6.79E-08)	*n.c.*
Mfap2	Microfibrillar-associated protein 2	1.7 (1.55E-07)		*up*
Mfap4	Microfibrillar-associated protein 4	2.16 (6.04E-05)	0.42 (2.10E-07)	*up*
Mkx	Mohawk		0.52 (0.000198)	*n.c.*
P4ha1	Procollagen-proline, 2-oxoglutarate 4-dioxygenase, alpha 1 polypeptide		0.46 (5.38E-06)	*n.c.*
Prg4	Proteoglycan 4		1.76 (0.00061)	*up*
Scx	Scleraxis		0.505 (7.71E-05)	*n.c.*
Sfrp2	Frizzled-related protein 2	1.8 (9.77E-05)		*up*
Thbs1	Thrombospondin 1	0.588 (9.97E-05)	0.544 (0.00044)	*up*
Thbs2	Thrombospondin 2		0.56 (0.00054)	*up*
Tnmd	Tenomodulin		0.534 (0.000136)	*n.c.*

Figure 1. RNAseq analysis of skin and Achilles tendons from *Col5a1*$^{+/+}$ and *Col5a1*$^{+/Neo}$ mice. (**A**) DEGs in skin and Achilles tendons from *Col5a1*$^{+/Neo}$ mice compared with *Col5a1*$^{+/+}$ mice (FDR < 0.1, fold change < 0.6 or fold change >1.4). (**B**) Ingenuity Pathway Analysis (IPA) on DEGs from skin and Achilles tendons samples (FDR < 0.1) demonstrating the top diseases and disorders and the top upstream regulators enriched in the data (for skin and tendons, see supplementary data for full list). (**C**) List of selected DEGs (see supplementary data for full list) FDR = False Discovery Rate. FC = fold change; n.c/empty tab = not changed; up = upregulated; down = downregulated. *DEGs reported in heart scar tissue from mice deficient of *Col5a1* in cardiac fibroblasts as was reported by Yokota *et al.* (19). Dark gray marks upregulated genes and light gray marks downregulated genes.

this *Col5a1*$^{+/\Delta}$ model confirmed haploinsufficiency of Col5a1 protein, abnormal dermis thickness and density and abnormal skin collagen fibers as seen by electron microscopy (Supplementary Material, Fig. S1B–D). Skin of *Col5a1*$^{+/\Delta}$ demonstrated reduced tensile strength as was seen in *Col5a1*$^{+/Neo}$ model (data not shown). The consistency between the two models suggested there was no transcriptional interference in *Col5a1*$^{+/Neo}$ mice. The *Col5a1*$^{+/Neo}$ model was used to further confirm molecular findings of which some were also confirmed in *Col5a1*$^{+/\Delta}$ model (supplementary data).

Altered Lum and Tsp1 expression in *Col5a1* haploinsufficient mice

Among the genes that changed in both skin and tendons of *Col5a1*$^{+/Neo}$ mice, we further evaluated the expression levels of *Lum* and *Thbs1* as these two genes are directly associated with ECM homeostasis. Lum is a small leucine-rich proteoglycan produced by dermal fibroblasts and is abundant in skin. It has a role in collagen fibrillogenesis and *Lum*-null mice present with skin and tendon fragility and delayed wound healing (22,23). *Lum* messenger RNA (mRNA) levels were increased in *Col5a1*$^{+/Neo}$ mice skin and tendons and confirmed by quantitative reverse transcription-polymerase chain reaction (qRT-PCR) (Fig. 2A and B). Tsp1 is a matricellular glycoprotein with essential role in spatiotemporal cell function through modulating cell–matrix interaction (24,25). Tsp1 is known to inhibit angiogenesis and to activate latent Tgf-β. *Thbs1*-null mice display acute and chronic inflammatory pulmonary and pancreatic infiltrates, a mild spinal lordosis and an elevated number of circulating white blood cells, which was improved following treatment with Tsp1-derived peptide that activates latent Tgf-β (26). Skin of *Thbs1*-null mouse presents with paucity of dermal matrix, excessive dermal vascular density and delayed wound healing (27). RNAseq data in skin and Achilles tendon from *Col5a1*$^{+/Neo}$ mice showed a decrease in *Thbs1* expression in both tissues. RT-PCR studies showed a decreasing trend in mRNA levels in both tissues (Fig. 2C) and Tsp1 protein levels in skin and primary fibroblasts were decreased in *Col5a1*$^{+/Neo}$ mice when compared with controls (Fig. 2D and E). Low levels of Tsp1 were also demonstrated in full-thickness skin samples from *Col5a1*$^{+/\Delta}$ mice (Supplementary Material, Fig. S2). Interestingly, *Col5a1*$^{+/Neo}$ mice skin show similar properties to those of *Thbs1*-null mice with reduced density of dermal connective tissue and delayed wound healing (4,10), suggesting *Tsp1* to be a major contributor to the phenotype in classic EDS mice.

The effect of *Col5a1* haploinsufficiency on collagen cross-linking

Given the important structural role of Col5a1 in ECM, we asked whether collagen cross-linking is altered in the

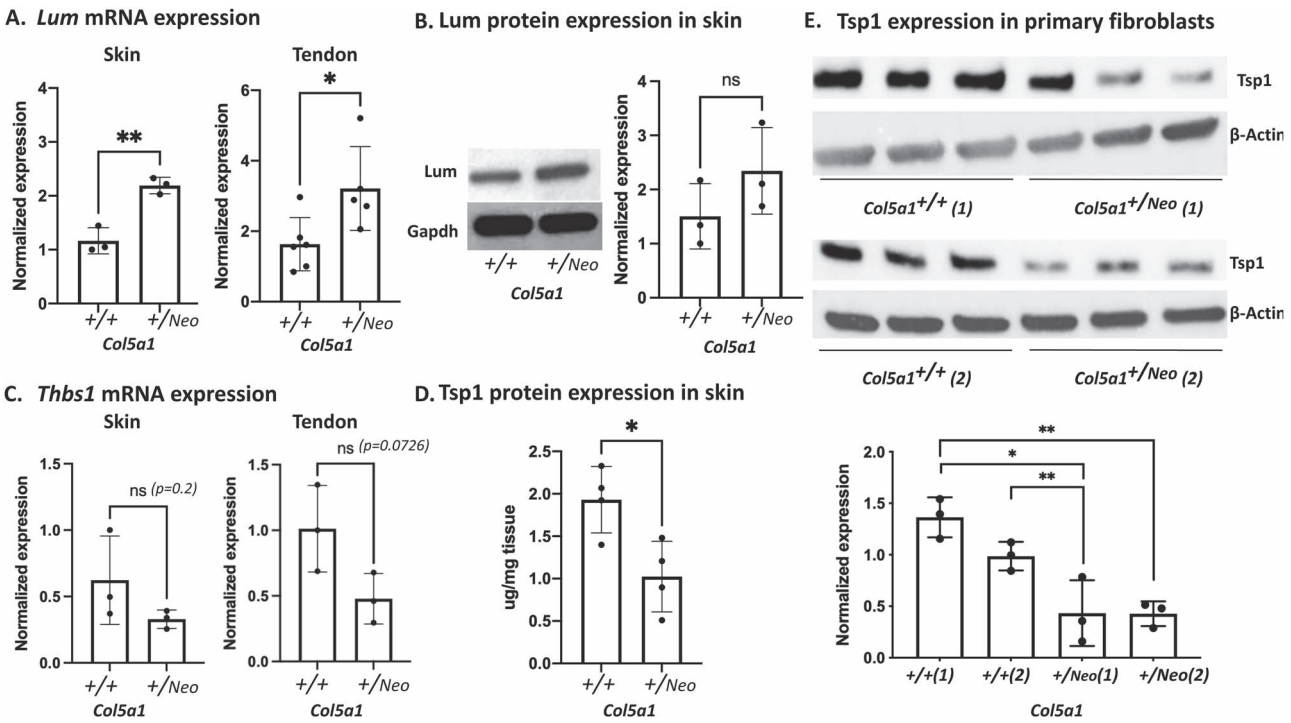

Figure 2. Changes in Lum and Thbs1/Tsp1 expression in *Col5a1*$^{+/Neo}$ mice skin and tendon. (**A**) *Lum* mRNA expression in skin and Achilles tendons ($n = 3$–6) using RT-PCR. (**B**) Lum protein expression in skin of *Col5a1*$^{+/+}$ and *Col5a1*$^{+/Neo}$ mice. (**C**) *Thbs1* mRNA expression in skin and Achilles tendons ($n = 3$) using RT-PCR. (**D**) Protein levels of Tsp1 in 4-week-old mice skin measured using immunoassay (ELISA) and normalized to total tissue protein. (**E**) Tsp1 protein levels in primary fibroblasts from *Col5a1*$^{+/Neo}$ skin. Western blot results and bands quantification. Three technical replicates were tested for each cell line. Statistically significant differences were assessed with one-way ANOVA for Tsp1 protein expression in skin (D) and with unpaired *t*-test for all other results $^{*}P < 0.05$; $^{**}P < 0.01$. cDNA levels were normalized to β2-microglobulin.

Col5a1$^{+/Neo}$ model. Our RNAseq data showed increased transcription levels of the key enzyme in collagen cross-linking, Lox (28), in skin from *Col5a1*$^{+/Neo}$ mice (Fig. 1C). RT-PCR studies confirmed this *Lox* mRNA increase in skin (Fig. 3A). Dermis from the skin of *Col5a1* haploinsufficient mice was treated with acetic acid to release fibrillar collagen molecules polymerized by aldimine cross-links. Quantification of the collagen molecules was done using reducing SDS-polyacrylamide gel electrophoresis (PAGE). Analysis of type I collagen cross-linking in skin from both *Col5a1*$^{+/Neo}$ and *Col5a1*$^{+/\Delta}$ mice revealed significant alterations in type I collagen fibers composition compared with control. The most consistent changes include a decrease in β1,2 dimers, cross-linked by an intramolecular aldol bond [between α1(I) and α2(I)] and increase in γ trimers, cross-linked by an intermolecular aldol bond [between α1(I) and α1(I)-α2(I)] (Fig. 3B). Similar alterations were observed in *Col5a1*$^{+/\Delta}$ mice (Supplementary Material, Fig. S3A) and may reflect the observed increase in large diameter collagen fibrils in skin of classic EDS mouse model. Interestingly, there were no significant changes in cross-linking of type I collagen identified in Achilles tendons from *Col5a1*$^{+/Neo}$ mice (Supplementary Material, Fig. S3B). This can be explained by tissue-specific variation in collagen cross-linking. Collagen structure in Achilles tendons is rich in hydroxylysine pyridinoline cross-linking bonds rather than in lysine aldehydes bonds as seen in skin (29) and therefore do not exhibit the same ratios between fibrillar collagen molecules on SDS-PAGE.

Increased Tgf-β expression in *Col5a1* haploinsufficient mice

Tgf-β is known to have a central role in skin homoeostasis and wound healing. It is an activator of fibroblasts and plays a major role in the induction of fibrosis (30). Its activity is context-dependent with temporospatial regulation throughout wound healing (31). Tgf-β dysregulation is involved in various wound pathologies. Given the clinical relevance of abnormal wound healing to classic EDS and the known effect of Tsp1 on activation of latent Tgf-β (32), we further investigated the expression of Tgf-β and its downstream effector, phosphorylated Smad2, in *Col5a1*$^{+/Neo}$ mice. Using enzyme-linked immunosorbent assay (ELISA), we found that Tgf-β expression was significantly higher in serum from male *Col5a1*$^{+/Neo}$ mice compared with controls (Fig. 4A). In the dermis of 8-week-old *Col5a1*$^{+/Neo}$ females, we found increased numbers of pSmad2-positive cells per dermis area by immunohistochemistry (IHC) staining (Fig. 4B and C). A similar increase in pSmad2-positive cells per dermis area was also seen in unwounded skin of *Col5a1*$^{+/\Delta}$ mice (Supplementary Material, Fig. S4). We demonstrate increased expression of the major Tgf-β effector in wound healing, alpha smooth muscle actin (αSma) (33), in Days 4 and 6 of full-thickness skin wound healing in

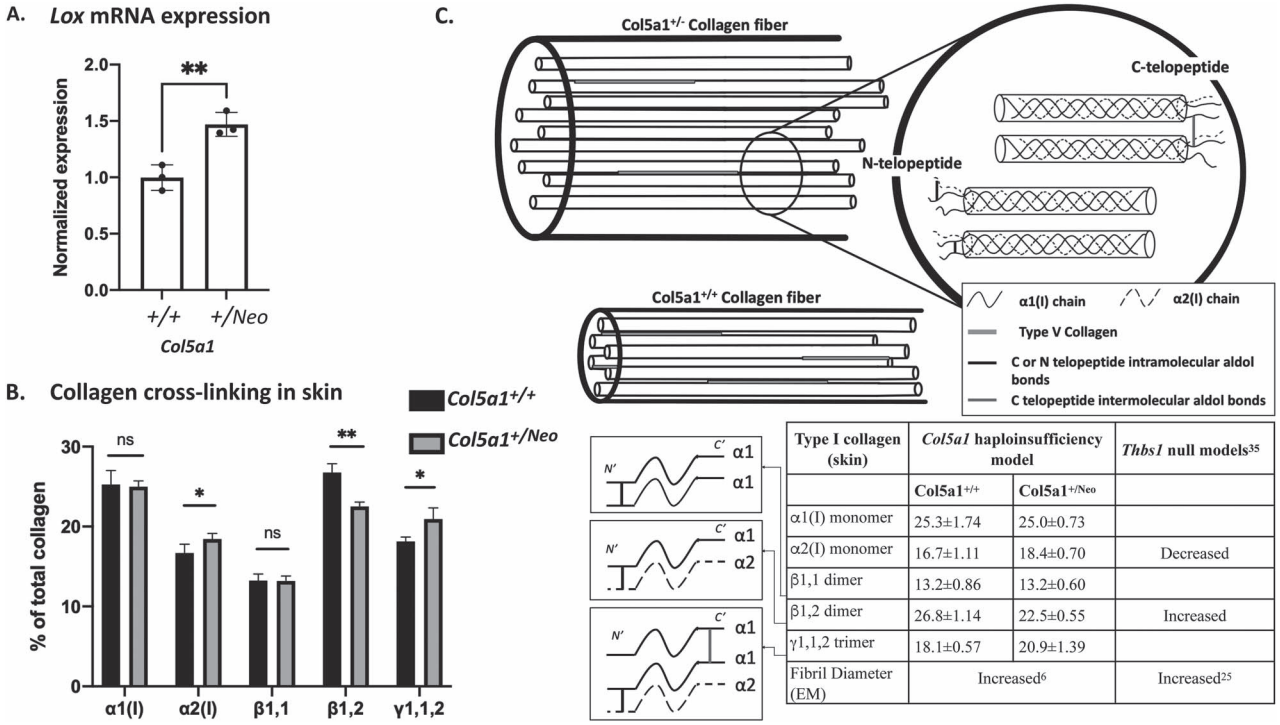

Type I collagen (skin)	*Col5a1* haploinsufficiency model		*Thbs1* null models[35]
	Col5a1$^{+/+}$	Col5a1$^{+/Neo}$	
α1(I) monomer	25.3±1.74	25.0±0.73	
α2(I) monomer	16.7±1.11	18.4±0.70	Decreased
β1,1 dimer	13.2±0.86	13.2±0.60	
β1,2 dimer	26.8±1.14	22.5±0.55	Increased
γ1,1,2 trimer	18.1±0.57	20.9±1.39	
Fibril Diameter (EM)	Increased[6]		Increased[25]

Figure 3. Lysyl oxidase expression levels and cross-linking studies in skin of *Col5a1*$^{+/Neo}$ versus *Col5a1*$^{+/+}$ mice. (**A**) mRNA expression of *Lox* in mice skin. β2-microglobulin was used as a loading control. (**B**) Cross-linking studies showing type I collagen distribution in skin of 11-week-old males *Col5a1*$^{+/Neo}$ versus *Col5a1*$^{+/+}$ mice ($n = 4$). Table presents cross-linking SDS-PAGE gel bands intensity quantification representing values of type I collagen distribution. Stated value are percentages of total type I collagen. *Thbs1*-null mice cross-linking studies in skin stated as published by Rosini *et al.* (35). (**C**) Schematic representation of type I collagen fibrils in classic EDS skin model versus control. For *P*-value calculation, unpaired *t*-test was used, two tail *P*-value was considered. *$P < 0.05$; **$P < 0.005$; ***$P < 0.0005$.

Col5a1$^{+/Neo}$ mice when compared with controls (Fig. 5). These results indicate elevation in both Tgf-β and its downstream signaling in skin of classic EDS mice, suggesting Tgf-β dysregulation may contribute to the pathological skin in this model.

Discussion

Treatment of connective tissue disorders of genetic etiology is challenging. Finding the key driving molecules is a critical step in disease-specific therapy development. Haploinsufficiency of a1(V) chain is the major cause of classic EDS. ColV is essential for type I collagen fibers nucleation and lateral expansion and complete knockout of *Col5a1* is embryonic lethal (6). Understanding the pathological mechanisms involved in the cells and the tissue's response to reduced levels of Col5a1 and abnormal type I collagen formation is essential for future development of innovative treatment options for classic EDS. In this work, we delineated some of the changes caused by *Col5a1* haploinsufficiency in a mouse model of classic EDS by transcriptomic approach. The use of full-thickness skin and Achilles tendon tissues emphasized the net result of transcription in the affected tissues compared with control. We showed the presence of gene expression pattern suggestive of chronic tissue injury using IPA analysis and demonstrating an overlap in gene expression with *Col5a1* deficient cardiac healing scar tissue. The increase in *Lox* expression (Fig. 3A) and in fibroblasts cellularity in classic EDS skin (Fig. 4C and Supplementary Material, Fig. S4B) gives additional evidence to increase skin ECM turnover. We showed increased Tgf-β and phosphorylated pSmad2 in the serum and the unwounded skin of classic EDS mouse model, respectively. We also showed increase Lum and decreased Tsp1 in skin and Achilles tendons of affected mice compared with control. Moreover, we characterized the cross-linking phenotype of type I collagen in haploinsufficient mice. Lastly, we established a new mouse model for classic EDS using CRISPR technology. This mouse model was verified and supports the existing model generated by Wenstrup *et al.* (6) and can be used for confirmatory future studies.

Transcriptome analysis of human fibroblasts from classic EDS patients revealed changes in expression of hundreds of genes when compared with control (20). In this work, we present transcriptome analysis of intact full-thickness skin samples from *Col5a1*$^{+/Neo}$ mouse model compared with control. We found a limited set of 30 genes to be differentially expressed. Interestingly, only few DEGs in our work were reported to be differentially expressed also in human classic EDS fibroblasts (20). This might not be surprising given the fact that the processes active at the tissue level include compensatory mechanisms that depend on the ECM and the various cell types in the tissue that do not exist in cultured fibroblasts. This can be supported by the significant overlap between the DEGs in our study and

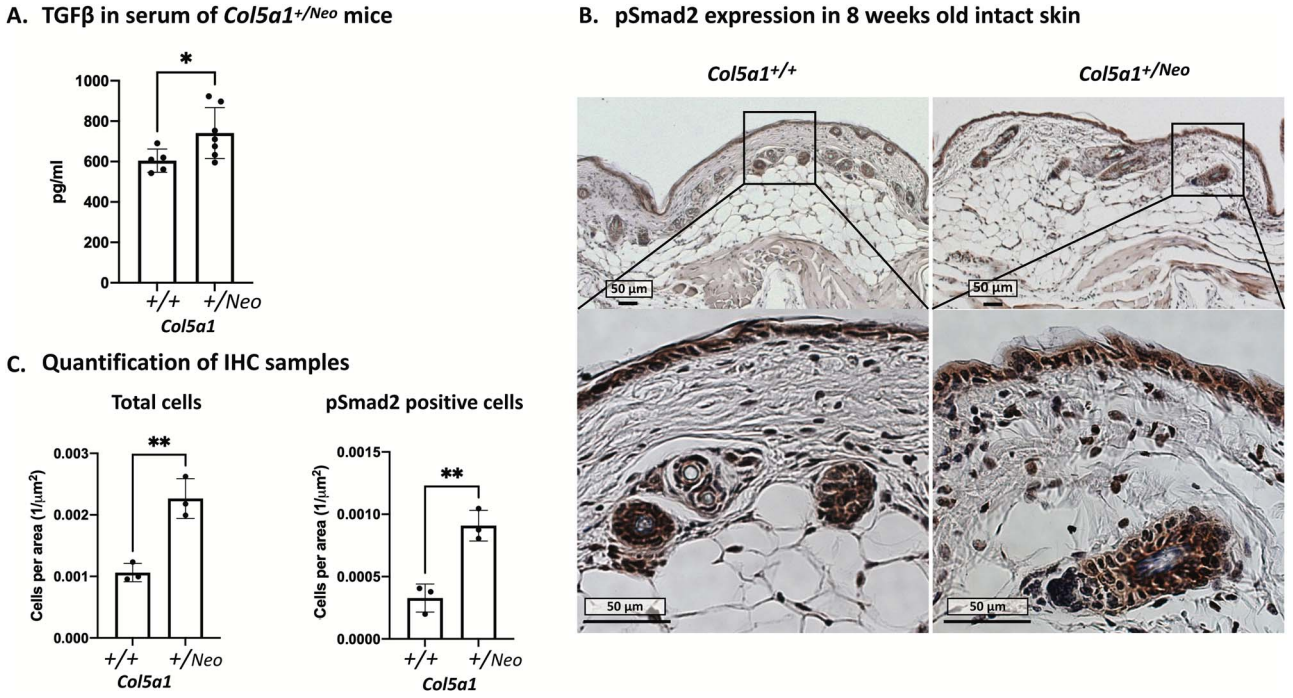

Figure 4. Tgf-β and pSmad2 are elevated in serum and unwounded skin from *Col5a1*$^{+/Neo}$ mouse model. (**A**) Tgf-β expression in the serum of *Col5a1*$^{+/Neo}$ versus *Col5a1*$^{+/+}$ male mice. Tgf-β levels were measured by immunoassay ($n = 5$–7). Statistically significance was assessed with one-way ANOVA. (**B**) pSmad2 expression in unwounded skin of 8-week-old females. (**C**) Quantification of total cells and pSmad2-positive cells per area in the dermis of 8-week-old females ($n = 3$, at least three different areas were evaluated in each slide). Black boxes delineate the magnified area. *$P < 0.05$; ** $P < 0.005$.

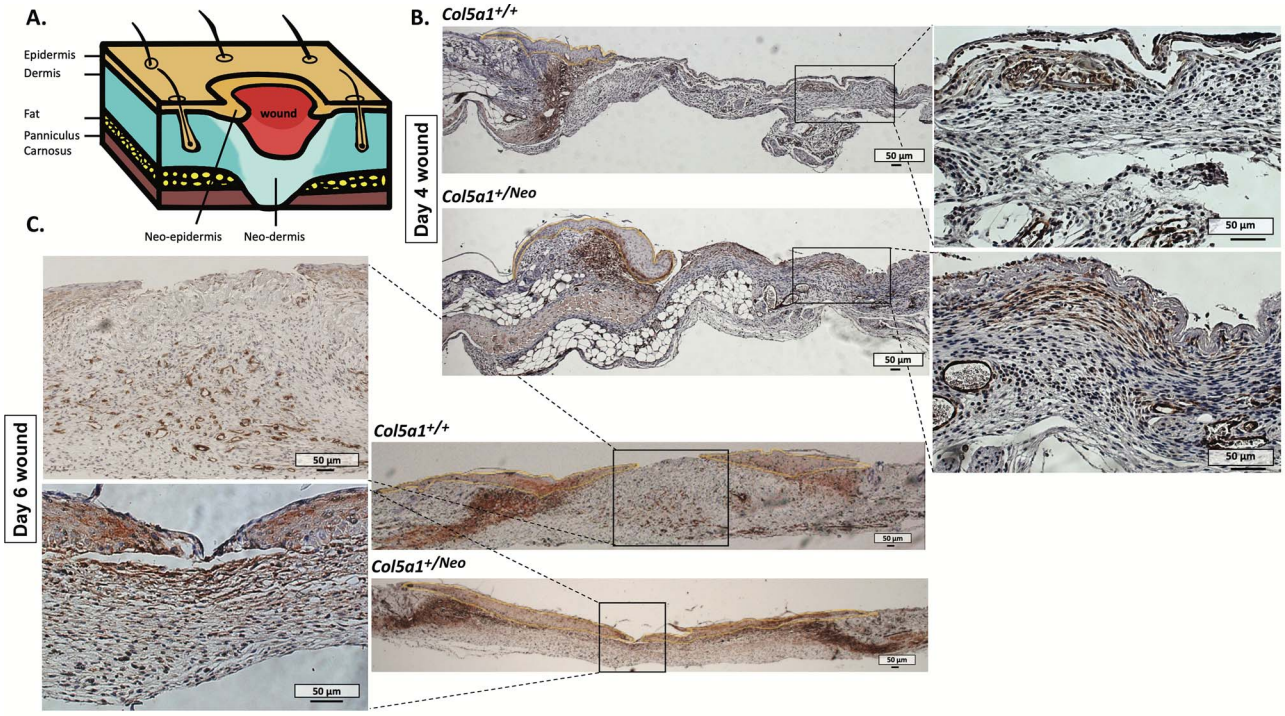

Figure 5. Smooth muscle actin (αSma) expression in Days 4 and 6 of full-thickness wound healing in skin of *Col5a1*$^{+/Neo}$ versus *Col5a1*$^{+/+}$ 8-week-old female mice. (**A**) Skin full-thickness wound schematics. (**B**, **C**) αSma immunohistochemistry in Day 4 (B) and Day 6 (C) of wound healing. Neo-epidermis at the wound's edge is outlined in yellow. Black boxes delineate the magnified area.

the DEGs expressed in myocardial ischemia-induced scar tissue from cardiac fibroblasts-specific *Col5a1* knockout mice (19). This overlap between an unwounded tissue (skin and tendon) and a healing tissue might suggest a constant active remodeling process in connective tissues of a *Col5a1* haploinsufficient mouse model. The normalization of collagen content in *Col5a1*$^{+/Neo}$ mice by 12 weeks of age supports the presence of efficient

A.

Skin Characteristics	*Col5a1* haploinsufficiency model	*Lum* null models	*Thbs1* null models
Dermal density	Decrease[4]	Decrease[22]	Decrease[26]
ECM organization	Disorganized[6]	Disorganized[22]	Disorganized[25]
Skin strength	Decrease[4]	Decrease[23]	Not described
Wound healing	Delayed[10]	Delayed[22]	Delayed[27]

B.

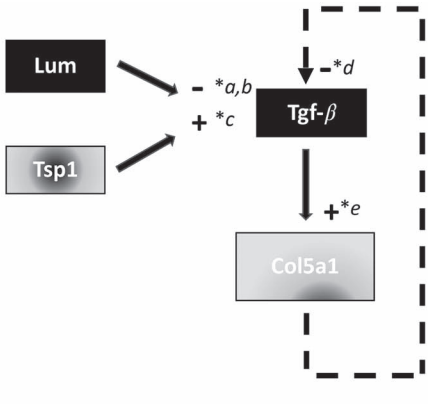

Figure 6. Summary of the effect of Col5a1, Lum and Tsp-1 deficiency on skin. (**A**) Table summarizing skin phenotype in *Col5a1*-haploinsufficient, *Lum*-null and *Thbs1*-null mice models. (**B**) Diagram describing regulation of Tgf-β, Lum and Tsp1 in response to *Col5a1* haploinsufficiency. '+/–' signs represent known interaction (see references). '+' for activation and '–' for inhibition; box color represents expression in skin of *Col5a1* haploinsufficient mouse according to the data presented in this work (black for increased expression and gray for decreased expression compared with control). Dashed arrow represents suggested upregulation effect (see text). *For references see *a,b*—Chen *et al.* (43), Botella *et al.* (44); *c*—Crawford *et al.* (26); *d*—Symoens *et al.* (11); *e*—Kahai *et al.* (39).

compensatory mechanisms to overcome the low collagen content in the skin in classic EDS mice model (4). The increased expression of Lum in *Col5a1*$^{+/Neo}$ mice skin and tendons might be part of this compensatory mechanism as Lum regulates fibrillogenesis, supports collagen fibrils organization and limits their lateral expansion (22), whereas *Lum*-null mice present skin laxity and fragility that overlap with the phenotype seen in EDS patients (34).

We identified Tsp1 to be downregulated in both skin and Achilles tendons of *Col5a1*$^{+/Neo}$ mice. *Thbs1*-null mice exhibit altered collagen cross-linking with decrease in total Lox but with increase in Lox activation. *In vitro* studies showed that Tsp1 regulates cross-linking through multiple mechanisms including binding to pro-Lox and inhibiting its activation (35). Although both *Thbs1*-null and *Col5a1*$^{+/Neo}$ mice present large diameter type I collagen fibrils, fragile skin and delayed wound healing (Fig. 6A), studies of skin from the two models present different cross-linking patterns (Fig. 3B). Although *Thbs1*-null mice present increase in the dimer β1,2 in the skin (35), *Col5a1*$^{+/Neo}$ mice present with opposite findings. This suggests that the common final result of large diameter fibrils is caused by different mechanisms. Unlike in the cornea where a high ratio of collagen type V to type I (1:5–1:10 versus 1:20–1:50 in other connective tissues) promotes synthesis of small diameter fibrils (5,36), haploinsufficiency of ColV in classic EDS mice leads to generation of large diameter collagen fibrils both in skin and tendons (4). Increase in fibril diameter results in a decreased ratio between the fibril surface and total molecules in cross-sections, which can explain the higher abundance of intermolecular C-telopeptide aldol trimers (higher γ112) and hence fewer dimers (lower β12). We interpret the cross-linking pattern in the *Col5a1* haploinsufficient mice to reflect the abundance of large type I collagen fibrils that are caused directly by the deficiency in ColV and does not reflect a primary defect in the cross-linking mechanism.

Increased Tgf-β activity has been shown to be involved in the pathogenicity of several connective tissue disorders. Its levels are increased in the serum of patients with EDS type IV, which is caused by haploinsufficiency of Type III collagen (37). Tgf-β dysregulation is involved in various wound healing pathologies. Tgf-β deficiency in the late phases of wound healing is associated with chronic wound, whereas its increased expression causes excessive fibrosis and hypertrophic scars (30). The abnormal wound healing phenotype in classic EDS is suggestive of Tgf-β dysregulation with differential impact on early versus late phases of wound healing. In this study, we show overexpression of Tgf-β in *Col5a1*$^{+/Neo}$ mice serum as well as increase in pSmad2 in unwounded skin. When comparing full-thickness wound healing between classic EDS mouse model and controls, we show increase in αSma expression. Fibroblasts differentiation to myofibroblasts expressing αSma is a key event in wound healing and is driven by Tgf-β (33). Myofibroblasts contribute to wound contractility and to production of ECM proteins. Prolonged myofibroblast activation in the healing wound contributes to the formation of hypertrophic scars (38).

It was demonstrated before that *N*-terminus of ColV directly binds Tgf-β (11) suggesting that ColV contributes to the regulation of Tgf-β in the ECM. Multiple evidences support the regulation of Col5a1 levels by Tgf-β. Tgf-β was shown to increase expression of Col5a1 during osteogenesis (39), in breast invasive ductal carcinoma (40) and in rat hematopoietic stem cell culture (41). Tsp1 is a known activator of Tgf-β and its low expression level in the presence of high levels of Tgf-β in our study suggests that this downregulation of Tsp1 is secondary to high Tgf-β levels in a negative feedback loop (Fig. 6B). Additional studies are required to delineate the effect of *Col5a1* haploinsufficiency on upregulation of Tgf-β in this model. Manipulating TGF-β levels in classic EDS can be considered as a therapeutic approach for classic EDS manifestations in unwounded skin and during wound

healing. Yet, the dynamic spatiotemporal expression of TGF-β and its multiple regulatory effects at the tissue level might impose challenges on this approach.

In conclusion, we provided global transcriptomic data of the critical disease-affected tissues, skin and tendon, from classic EDS mouse model and a new mouse model of *Col5a1* haploinsufficiency. For the identification of therapeutic strategies for this condition, additional studies are required to define which of the multiple molecular changes that we see is a primary pathology, contributing to the phenotype versus a secondary effect aiming to compensate for the initial insult. Attempts to reverse the latter could worsen the phenotype while reversing the effect of the first might rescue it. This work contributes to understanding the changes downstream of the *Col5a1* haploinsufficiency in classic EDS mouse model and can help to identify therapeutic targets in the future.

Materials and Methods

Mice and primary fibroblasts

Col5a1$^{+/Neo}$ C57BL/6 mice were a kind gift from Dr. David E. Birk (6). We generated *Col5a1*$^{+/\Delta}$ C57BL/6 mice using CRISPR/Cas9 system with sgRNA guide gaaattaatacgactcactataggCCTGGTCCACCAGGCCCCCGgttttagagctagaaatagc targeting exon 48 (target sequence was on the basis of pathogenic variant in Dr Lee's patient). Primary fibroblasts were grown from mice axillary skin using DMEM supplied with 10% FBS, 100 U ml^{-1} penicillin, 100 μg ml^{-1} streptomycin and 100 μm ascorbic acid. All mice were housed in the Baylor College of Medicine Animal Vivarium and animal experiments were performed following the approved protocol of the Animal Care and Use Committee at the Baylor College of Medicine.

RNA extraction and quantitative PCR

Skin and tendons were homogenized using TissueLyserII (Qiagen) in five cycles of 1 min each at 23 Hz. Total RNA was extracted from mice skin or cultured cells with TRIzol reagent (Invitrogen) and from tendons with Proteinase K. All extractions were completed with RNAeasy Fibrous Tissue kit (Qiagen). Complementary DNAs (cDNAs) were synthesized from extracted RNA with the Superscript III First Strand RT-PCR kit (Invitrogen) and qRT- PCR amplifications were performed in LightCycler (Roche). Murine β2-microglobulin or Gapdh were used as the internal control to normalize gene expression.

RNA-sequencing

Interscapular skin and Achilles tendons were collected from 4-week-old *Col5a1*$^{+/+}$ and *Col5a1*$^{+/Neo}$ males. Both Achilles tendons were used from each mouse. Total RNA was extracted by the same method used for qRT-PCR. mRNAs were captured by Dynabeads Oligo $(dT)_{25}$ magnetic beads (Invitrogen) and fragmented by using the NEBNext Magnesium RNA Fragmentation Module (New England Biolabs). Double-stranded cDNAs were synthesized with the SuperScript Double-Stranded cDNA Synthesis kit (Invitrogen) and used as the library template. Libraries were generated with the TruSeq RNA Library Preparation kit (Illumina). Sequencing was performed on an Illumina HiSeq 2000 instrument as 100 bp pair-end reads at the Human Genome Sequencing Center at Baylor College of Medicine (https://www.hgsc.bcm.edu). Raw reads were mapped to mouse genome mm9 and splice junction sites with bowtie (v0.12.7) and Tophat (v2.0.0) in the strand-specific model when the strand-specific library protocol was applied. The reference Mouse Genome annotation file (mm9) was downloaded from UCSC (http://genome.ucsc.edu/). Read counts mapped to each gene were calculated by HTseq (http://www-huber.embl.de) with the default model. Fragments per kilobase of exon model per million fragments mapped values were calculated using Cufflinks (version 2.1.1, http://cufflinks.cbcb.umd.edu). Differential expression was analyzed with R (v2.14.0, http://www.R-project.org) and Bioconductor (release 2.10) with the R package DESeq (v1.6.0). Pathways and upstream regulator analyses were performed by IPA (http://www.ingenuity.com/) with default parameters.

Enzyme-linked immunosorbent assay

To detect TGF-β1 level in serum from *Col5a1*$^{+/Neo}$ versus *Col5a1*$^{+/+}$, mice blood was collected by retro-orbital bleeding from male mice 1–3 months old. Serum extraction and detection procedure were completed according to the manufacturer's recommendation in the TGF-beta 1 Quantikine ELISA kit (R&D systems, DB100B). We did not activate latent TGF-β prior to measurement. To detect Tsp1 levels in skin, we used Mouse THBS1/Tsp1 (sandwich ELISA) ELISA kit (LS-F12876). Skin was collected from 4-week-old mice and was processed according to the manufacture's recommendations. Tsp1 levels were normalized to protein concentration, which was measured using Micro BCA reagent (Pierce).

Immunoblotting

Protein was extracted using RIPA buffer (50 mM Tris, 150 mM NaCl, 0.1% SDS, 0.5% sodium deoxycholate, 1% triton) and total protein concentration of the lysate was measured with Micro BCA reagent (Pierce) following the manufacturer's instructions. Protein was suspended in laemmeli buffer containing 5% β-mercaptoethanol and separated on Mini Protean TGX SDS-PAGE gel (gradient 4–20% or 10%; Bio-Rad) and transferred onto PVDF membrane for western blot analysis. Membranes were incubated with anti-Lum (Abcam, ab168348), anti-Tsp1 (Invitrogen, MA5–13398) and anti-GAPDH (Sigma, 69 295) antibodies. Anti-Col5a1 antibody was a kind gift from Dr David E. Birk (6). Alternatively, anti-Col5a1 antibody from Santa Cruz (H-200, sc-20 648) was used. Secondary HRP-linked anti-rabbit or anti-mouse antibodies were used.

Signal was detected with the ECL plus western blotting detection system (GE). X-ray films were scanned, and the density of each band was quantified using ImageJ software (National Institutes of Health).

Immunostaining and histology

For immunohistochemistry, we collected healthy mice skin. Skin was fixed for 48 h in 4% paraformaldehyde shaking in 4°C and embedded in paraffin. After deparaffinization and rehydration, we performed heat-induced antigen retrieval (Dako, S1700). Endogenous peroxidase was blocked using 3% hydrogen peroxide for 10 min. After incubation with blocking solution (3% normal goat serum, 0.1% BSA, 0.1% Triton X-100 in phosphate-buffered saline), we incubated sections in primary antibodies for overnight in 4°C. Anti-pSmad 2 (Invitrogen, 40–0800) and anti-αSma (Abcam, ab5694). Appropriate secondary antibody was used for 1 h at room temperature. Substrate DAB was used according to the manufacturer's recommendations and followed with eosin staining, dehydrated and mounting using Cytoseal XYL xylene-based mounting medium (Thermo Scientific). Images were taken with a light microscope (Axioplan 2, Zeiss) using identical exposure times for WT and mutant littermates.

Collagen extraction and cross-linking studies

All tissues were washed in saline and skin was defatted in 50:50 chloroform:methanol before lyophilizing to get dry weight. Each sample of 2–4 mg was acid extracted in 1 ml 3% acetic acid at 4°C for 24 h. The dried extracts were dissolved in SDS-PAGE sample buffer at 5 mg/ml using initial dry weight. Equal loads were run on 6% SDS-PAGE. ImageJ software was used for densitometry analysis.

Wound-healing studies

Full-thickness wounds were done on the back of 8-week-old females mice in a method modified from to previously published protocol (42). In brief, hair on the mouse back was chemically removed (Nair). Two full-thickness wounds were generated on the mouse' back at the subscapular area using 5-mM biopsy punch (Miltex). Wounds were stabilized using a sterile ring-shaped 0.5 mM thick silicon splint (Grace Bio-Labs, 664 571) with an inner diameter of 6 mM. Each splint was fixed to the mouse's skin using silicone glue (KRYOLAN) and three sutures. The wounds were covered with 3 M TegadermTM film. Buprenorphine SR, 1 mg/ml (ZooPharm Cat. No.: BZ8069317), was used for analgesia and was given before surgery.

Statistical analysis

All statistical analyses used parametric unpaired tests including one-way analysis of variance (ANOVA) or *t*-tests. Prism-9 GraphPad (https://www.graphpad.com/scientific-software/prism/) was used to perform statistical analysis. One-way ANOVA was performed to assess the statistically significant differences between the levels of Tgf-β in the serum and between the levels of Tsp1 in the skin of *Col5a1*$^{+/+}$ and *Col5a1*$^{+Neo}$ mice. All other statistically significant differences were assessed with unpaired *t*-test. *P*-values < 0.05 were considered significant.

Supplementary Material

Supplementary Material is available at *HMG* online.

Conflict of Interest statement. None declared.

Funding

The Pamela and David Ott Center of Excellence for Heritable Disorders of Connective Tissue at Baylor College of Medicine, by the Eunice Kennedy Shriver National Institute of Child Health and Human Development of the National Institutes of Health (Award Number P50HD103555) for use of the Core facilities. The BCM Advanced Technology Cores with funding from the National Institutes of Health (AI036211, CA125123, DK056338); the Rolanette and Berdon Lawrence Bone Disease Program of Texas and the BCM Center for Skeletal Medicine and Biology and the Pamela and David Ott Center for Heritable Disorders of Connective Tissue.

References

1. Bowen, J.M., Sobey, G.J., Burrows, N.P., Colombi, M., Lavallee, M.E., Malfait, F. and Francomano, C.A. (2017) Ehlers-Danlos syndrome, classical type. *Am. J. Med. Genet. C Semin. Med. Genet.*, **175**, 27–39.
2. Ritelli, M., Venturini, M., Cinquina, V., Chiarelli, N. and Colombi, M. (2020) Multisystemic manifestations in a cohort of 75 classical Ehlers-Danlos syndrome patients: natural history and nosological perspectives. *Orphanet J. Rare Dis.*, **15**, 197.
3. Birk, D.E. (2001) Type V collagen: heterotypic type I/V collagen interactions in the regulation of fibril assembly. *Micron*, **32**, 223–237.
4. Wenstrup, R.J., Florer, J.B., Davidson, J.M., Phillips, C.L., Pfeiffer, B.J., Menezes, D.W., Chervoneva, I. and Birk, D.E. (2006) Murine model of the Ehlers-Danlos syndrome. col5a1 haploinsufficiency disrupts collagen fibril assembly at multiple stages. *J. Biol. Chem.*, **281**, 12888–12895.
5. Wenstrup, R.J., Florer, J.B., Cole, W.G., Willing, M.C. and Birk, D.E. (2004) Reduced type I collagen utilization: a pathogenic mechanism in COL5A1 haplo-insufficient Ehlers-Danlos syndrome. *J. Cell. Biochem.*, **92**, 113–124.
6. Wenstrup, R.J., Florer, J.B., Brunskill, E.W., Bell, S.M., Chervoneva, I. and Birk, D.E. (2004) Type V collagen controls the initiation of collagen fibril assembly. *J. Biol. Chem.*, **279**, 53331–53337.
7. Johnston, J.M., Connizzo, B.K., Shetye, S.S., Robinson, K.A., Huegel, J., Rodriguez, A.B., Sun, M., Adams, S.M., Birk, D.E. and Soslowsky, L.J. (2017) Collagen V haploinsufficiency in a murine model of classic Ehlers-Danlos syndrome is associated with deficient structural and mechanical healing in tendons. *J. Orthop. Res.*, **35**, 2707–2715.
8. Connizzo, B.K., Han, L., Birk, D.E. and Soslowsky, L.J. (2016) Collagen V-heterozygous and -null supraspinatus tendons exhibit altered dynamic mechanical behaviour at multiple hierarchical scales. *Interface Focus*, **6**, 20150043.

9. Sun, M., Connizzo, B.K., Adams, S.M., Freedman, B.R., Wenstrup, R.J., Soslowsky, L.J. and Birk, D.E. (2015) Targeted deletion of collagen V in tendons and ligaments results in a classic Ehlers-Danlos syndrome joint phenotype. *Am. J. Pathol.*, **185**, 1436–1447.
10. DeNigris, J., Yao, Q., Birk, E.K. and Birk, D.E. (2016) Altered dermal fibroblast behavior in a collagen V haploinsufficient murine model of classic Ehlers-Danlos syndrome. *Connect. Tissue Res.*, **57**, 1–9.
11. Symoens, S., Renard, M., Bonod-Bidaud, C., Syx, D., Vaganay, E., Malfait, F., Ricard-Blum, S., Kessler, E., Van Laer, L., Coucke, P. *et al.* (2011) Identification of binding partners interacting with the alpha1-N-propeptide of type V collagen. *Biochem. J.*, **433**, 371–381.
12. Zoppi, N., Gardella, R., De Paepe, A., Barlati, S. and Colombi, M. (2004) Human fibroblasts with mutations in COL5A1 and COL3A1 genes do not organize collagens and fibronectin in the extracellular matrix, down-regulate alpha2beta1 integrin, and recruit alphavbeta3 instead of alpha5beta1 integrin. *J. Biol. Chem.*, **279**, 18157–18168.
13. Zoppi, N., Chiarelli, N., Ritelli, M. and Colombi, M. (2018) Multifaced roles of the alphavbeta3 integrin in Ehlers-Danlos and arterial tortuosity Syndromes' dermal fibroblasts. *Int. J. Mol. Sci.*, **19**, 982.
14. Coker, R.K., Laurent, G.J., Shahzeidi, S., Lympany, P.A., du Bois, R.M., Jeffery, P.K. and McAnulty, R.J. (1997) Transforming growth factors-beta 1, –beta 2, and -beta 3 stimulate fibroblast procollagen production in vitro but are differentially expressed during bleomycin-induced lung fibrosis. *Am. J. Pathol.*, **150**, 981–991.
15. Gasparini, G., Cozzani, E. and Parodi, A. (2020) Interleukin-4 and interleukin-13 as possible therapeutic targets in systemic sclerosis. *Cytokine*, **125**, 154799.
16. Li, R. and Frangogiannis, N.G. (2021) Chemokines in cardiac fibrosis. *Curr. Opin. Physio.*, **19**, 80–91.
17. Cheng, J., Wang, Y., Wang, D. and Wu, Y. (2013) Identification of collagen 1 as a post-transcriptional target of miR-29b in skin fibroblasts: therapeutic implication for scar reduction. *Am. J. Med. Sci.*, **346**, 98–103.
18. Guo, J., Lin, Q., Shao, Y., Rong, L. and Zhang, D. (2017) miR-29b promotes skin wound healing and reduces excessive scar formation by inhibition of the TGF-beta1/Smad/CTGF signaling pathway. *Can. J. Physiol. Pharmacol.*, **95**, 437–442.
19. Yokota, T., McCourt, J., Ma, F., Ren, S., Li, S., Kim, T.H., Kurmangaliyev, Y.Z., Nasiri, R., Ahadian, S., Nguyen, T. *et al.* (2020) Type V collagen in scar tissue regulates the size of scar after heart injury. *Cell*, **182**, 545–562 e523.
20. Chiarelli, N., Carini, G., Zoppi, N., Ritelli, M. and Colombi, M. (2019) Molecular insights in the pathogenesis of classical Ehlers-Danlos syndrome from transcriptome-wide expression profiling of patients' skin fibroblasts. *PLoS One*, **14**, e0211647.
21. Pham, C.T., MacIvor, D.M., Hug, B.A., Heusel, J.W. and Ley, T.J. (1996) Long-range disruption of gene expression by a selectable marker cassette. *Proc. Natl. Acad. Sci. U. S. A.*, **93**, 13090–13095.
22. Yeh, J.T., Yeh, L.K., Jung, S.M., Chang, T.J., Wu, H.H., Shiu, T.F., Liu, C.Y., Kao, W.W. and Chu, P.H. (2010) Impaired skin wound healing in lumican-null mice. *Br. J. Dermatol.*, **163**, 1174–1180.
23. Chakravarti, S. (2002) Functions of lumican and fibromodulin: lessons from knockout mice. *Glycoconj. J.*, **19**, 287–293.
24. Bornstein, P. (2001) Thrombospondins as matricellular modulators of cell function. *J. Clin. Invest.*, **107**, 929–934.
25. Kim, D.J., Christofidou, E.D., Keene, D.R., Hassan Milde, M. and Adams, J.C. (2015) Intermolecular interactions of thrombospondins drive their accumulation in extracellular matrix. *Mol. Biol. Cell*, **26**, 2640–2654.
26. Crawford, S.E., Stellmach, V., Murphy-Ullrich, J.E., Ribeiro, S.M., Lawler, J., Hynes, R.O., Boivin, G.P. and Bouck, N. (1998) Thrombospondin-1 is a major activator of TGF-beta1 in vivo. *Cell*, **93**, 1159–1170.
27. Agah, A., Kyriakides, T.R., Lawler, J. and Bornstein, P. (2002) The lack of thrombospondin-1 (TSP1) dictates the course of wound healing in double-TSP1/TSP2-null mice. *Am. J. Pathol.*, **161**, 831–839.
28. Yang, N., Cao, D.F., Yin, X.X., Zhou, H.H. and Mao, X.Y. (2020) Lysyl oxidases: emerging biomarkers and therapeutic targets for various diseases. *Biomed. Pharmacother.*, **131**, 110791.
29. Hudson, D.M., Archer, M., Rai, J., Weis, M.A., Fernandes, R.J. and Eyre, D.R. (2021) Age-related type I collagen modifications reveal tissue-defining differences between ligament and tendon. *Matrix Biol. Plus*, **12**, 100070.
30. Kiritsi, D. and Nystrom, A. (2018) The role of TGFbeta in wound healing pathologies. *Mech. Ageing Dev.*, **172**, 51–58.
31. Finnson, K.W., McLean, S., Di Guglielmo, G.M. and Philip, A. (2013) Dynamics of transforming growth factor Beta Signaling in wound healing and scarring. *Adv. Wound Care*, **2**, 195–214.
32. Atanasova, V.S., Russell, R.J., Webster, T.G., Cao, Q., Agarwal, P., Lim, Y.Z., Krishnan, S., Fuentes, I., Guttmann-Gruber, C., McGrath, J.A. *et al.* (2019) Thrombospondin-1 is a major activator of TGF-beta Signaling in recessive dystrophic epidermolysis bullosa fibroblasts. *J. Invest. Dermatol.*, **139**, 1497–1505.e5.
33. Tomasek, J.J., Gabbiani, G., Hinz, B., Chaponnier, C. and Brown, R.A. (2002) Myofibroblasts and mechano-regulation of connective tissue remodelling. *Nat. Rev. Mol. Cell Biol.*, **3**, 349–363.
34. Chakravarti, S., Magnuson, T., Lass, J.H., Jepsen, K.J., LaMantia, C. and Carroll, H. (1998) Lumican regulates collagen fibril assembly: skin fragility and corneal opacity in the absence of lumican. *J. Cell Biol.*, **141**, 1277–1286.
35. Rosini, S., Pugh, N., Bonna, A.M., Hulmes, D.J.S., Farndale, R.W. and Adams, J.C. (2018) Thrombospondin-1 promotes matrix homeostasis by interacting with collagen and lysyl oxidase precursors and collagen cross-linking sites. *Sci. Signal.*, **11**, eaar2566.
36. Sun, M., Chen, S., Adams, S.M., Florer, J.B., Liu, H., Kao, W.W., Wenstrup, R.J. and Birk, D.E. (2011) Collagen V is a dominant regulator of collagen fibrillogenesis: dysfunctional regulation of structure and function in a corneal-stroma-specific Col5a1-null mouse model. *J. Cell Sci.*, **124**, 4096–4105.
37. Morissette, R., Schoenhoff, F., Xu, Z., Shilane, D.A., Griswold, B.F., Chen, W., Yang, J., Zhu, J., Fert-Bober, J., Sloper, L. *et al.* (2014) Transforming growth factor-beta and inflammation in vascular (type IV) Ehlers-Danlos syndrome. *Circ. Cardiovasc. Genet.*, **7**, 80–88.
38. Van De Water, L., Varney, S. and Tomasek, J.J. (2013) Mechanoregulation of the myofibroblast in wound contraction, scarring, and fibrosis: opportunities for new therapeutic intervention. *Adv. Wound Care*, **2**, 122–141.
39. Kahai, S., Vary, C.P., Gao, Y. and Seth, A. (2004) Collagen, type V, alpha1 (COL5A1) is regulated by TGF-beta in osteoblasts. *Matrix Biol.*, **23**, 445–455.
40. Ren, W., Zhang, Y., Zhang, L., Lin, Q., Zhang, J. and Xu, G. (2018) Overexpression of collagen type V alpha1 chain in human breast invasive ductal carcinoma is mediated by TGF-beta1. *Int. J. Oncol.*, **52**, 1694–1704.

41. Mak, K.M., Png, C.Y. and Lee, D.J. (2016) Type V collagen in health, disease, and fibrosis. *Anat. Rec.*, **299**, 613–629.
42. Wang, X., Ge, J., Tredget, E.E. and Wu, Y. (2013) The mouse excisional wound splinting model, including applications for stem cell transplantation. *Nat. Protoc.*, **8**, 302–309.
43. Chen, S.W., Tung, Y.C., Jung, S.M., Chu, Y., Lin, P.J., Kao, W.W. and Chu, P.H. (2017) Lumican-null mice are susceptible to aging and isoproterenol-induced myocardial fibrosis. *Biochem. Biophys. Res. Commun.*, **482**, 1304–1311.
44. Botella, L.M., Sanz-Rodriguez, F., Sanchez-Elsner, T., Langa, C., Ramirez, J.R., Vary, C., Roughley, P.J. and Bernabeu, C. (2004) Lumican is down-regulated in cells expressing endoglin. Evidence for an inverse correlationship between endoglin and lumican expression. *Matrix Biol.*, **22**, 561–572.